

Impacts of reaction and curing conditions on polyamide composite reverse osmosis membrane properties

Asim K. Ghosh, Byeong-Heon Jeong, Xiaofei Huang, Eric M.V. Hoek*

Civil & Environmental Engineering Department and Water Technology Research Center, University of California, Los Angeles (UCLA), Los Angeles, CA 90095-1593, USA

Received 14 July 2007; received in revised form 21 November 2007; accepted 25 November 2007
Available online 4 December 2007

Abstract

Here we report on the impacts of organic solvent properties, reaction conditions, and curing conditions on polyamide composite reverse osmosis membrane separation performance, film structure, and interfacial properties. We provide direct experimental evidence that: (1) MPD diffusivity in the organic phase governs MPD–TMC thin film water permeability, (2) MPD diffusivity and solubility influence MPD–TMC thin film crosslinking in competing ways, (3) water permeability correlates most strongly with MPD–TMC film structure (i.e., crosslinking), and (4) salt rejection correlates most strongly with MPD–TMC film thickness and morphology. Overall, higher flux membranes with good salt rejection appear to comprise thinner, more heavily crosslinked film structures. Such high performance RO membranes are obtained by (1) selecting high surface tension, low viscosity solvents, (2) controlling protonation of MPD and hydrolysis of TMC during interfacial polymerization, and (3) optimizing curing temperature and time based on organic solvent volatility. Finally, although more research is necessary, our results suggest the rugose morphology and relative hydrophobicity of high performance MPD–TMC membranes might enhance concentration polarization and exacerbate surface fouling.
© 2007 Elsevier B.V. All rights reserved.

Keywords: Reverse osmosis; Polyamide; Thin film composite; Interfacial polymerization; Desalination

1. Introduction

Modern reverse osmosis (RO) membranes are formed as flat sheets or hollow fibers comprising an ultra-thin polyamide film coated over a porous polysulfone support membrane [1,2]. The selective polyamide barrier layer is formed *in situ* by polycondensation reaction of polyfunctional amine and acid chloride monomers at the interface of two immiscible solvents. These elegantly engineered materials exhibit excellent performance in many desalination and water purification applications; however, significant interest remains in discovering more energy-efficient, contaminant-selective, and fouling-resistant versions of these membranes. Tailoring separation performance and interfacial properties of RO membranes requires understanding, at a fundamental level, the mechanisms governing thin film formation.

In forming a polyamide thin film, a polyfunctional amine is dissolved in water and a polyfunctional acid chloride is dissolved in apolar organic solvents like hexane, naphtha, cyclohexane, freon, or isoparaffin [3–5]. When the two monomer solutions are brought into contact, both monomers partition across the liquid–liquid interface and react to form a polymer; however, polymerization occurs predominantly in the organic phase due to the relatively low solubility of most acid chlorides in water [6–8]. Therefore, it is common to use a large excess of amine over acid chloride (typically about 20:1), which drives partitioning and diffusion of the amine into the organic phase. Any factors that alter the solubility and diffusivity of the amine monomer in the organic phase affect the reaction rate, and thus, the morphology and structure of the resulting polyamide film, which ultimately define separation performance and interfacial properties [8,9].

Selecting the organic solvent is critical since it governs, at a minimum, the amine monomer solubility and diffusivity in the reaction zone. For example, one recent study demonstrated that hexane and isopar produced significantly different TFC membranes, where isopar produced RO membranes with smaller

* Corresponding author at: Civil & Environmental Engineering Department, 5732-G Boelter Hall, P.O. Box 951593, University of California, Los Angeles (UCLA), Los Angeles, CA 90095-1593, USA. Tel.: +1 310 206 3735; fax: +1 310 206 2222.

E-mail address: hoek@seas.ucla.edu (E.M.V. Hoek).

apparent pore size [10]. Solvent properties and reaction conditions (particularly temperature) affect the density, viscosity, and surface tension of the organic solvent. Viscosity clearly influences diffusion; however, solvent surface tension controls the amine solubility and, as a consequence, the amine-to-acid chloride concentration ratio in the reaction zone and the degree of polymerization. Organic solvent surface tension also governs miscibility of the two liquid phases (particularly penetration of the organic phase by water), which might alter hydrolysis and protonation states of acid chloride and amine moieties and the extent of crosslinking.

It is common in practice to use combinations of additives to influence monomer solubility, diffusivity, hydrolysis, or protonation or to scavenge inhibitory reaction byproducts. For example, addition of small amounts of hydrophilic water-soluble polymers or a polyhydric alcohol to the amine solution can produce high-flux reverse osmosis membranes with good rejection [11]. In a patent issued to Chau [3], aprotic solvents like *N,N*-dimethylformamide (DMF) are added to the aqueous aromatic amine solution. Initially, DMF reacts with an acyl chloride to produce an amidinium chloride, which is relatively unreactive toward aromatic amines. Later the amidinium chloride hydrolyzes to a carboxylate group, which inhibits crosslinking and produces more negative charge and higher water flux.

Adding dimethyl sulfoxide (DMSO) to the aqueous amine solution increases the miscibility of water and hexane and probably also enhances MPD diffusivity, ultimately, improving water flux by formation of a thinner polyamide film [12,13]. Increased water–organic miscibility may cause hydrolysis of acid chlorides or de-protonation of amines, thereby reducing their reactivity and the extent of crosslinking. These authors report that surface roughness and surface area of these membranes increase as the concentration of DMSO increases, which suggests a correlation between surface roughness and permeability.

Sodium hydroxide, sodium tertiary phosphate, dimethyl piperazine, triethylamine (TEA), and other acylation catalysts accelerate the MPD–TMC reaction by removing hydrogen halides formed during amide bond formation [2]. It is suggested that the strength of the acid acceptor affects the degree of concurrent hydrolysis, and hence, membrane structure and performance. The aqueous solution may further contain a surfactant or organic acids like camphor sulfonic acid (CSA) improve absorption of the amine solution in the support [14,15].

Most studies of the MPD–TMC system indicate that curing is a necessary step to stabilize polyamide thin films [16,17]. Heat curing is used after film formation to remove residual organic solvent from the film and to promote additional crosslinking through dehydration of amine and carboxylic acid residues. This tends to increase water flux and salt rejection. With increase in curing time or temperature, the porosity of the polyamide film is reduced by crosslinking. This is accompanied by significant decrease in water flux, but increase in salt rejection. However, exposure to high curing temperatures or long curing times can damage the microporous skin layer of the support membrane,

which tends to decrease both water flux and salt rejection. Generally, curing temperatures ranging from 40 to 120 °C are used [18].

In this paper, we attempt to correlate MPD–TMC reaction and curing conditions to RO membrane separation performance (water flux, salt rejection), film structure (crosslinking, thickness), and interfacial characteristics (hydrophilicity, roughness). Four organic solvents are selected to produce wide variations in MPD solubility and diffusivity. We also evaluate the addition of the salt of TEA and CSA to the aqueous MPD solution and the impacts of organic–TMC solution temperature. These experiments allow us to satisfy our primary objective, that is, to elucidate the various interrelationships among reaction conditions and membrane properties. Finally, we evaluate the impacts of curing temperature and time on the properties of membranes formed in a few different organic solvents.

2. Experimental

2.1. Chemicals and reagents

Polysulfone (PSf) transparent beads with number average molecular weight of 26,000 Da (Sigma–Aldrich, Milwaukee, WI, USA), *N*-methyl pyrrolidone (NMP) (reagent grade, Acros Organics, USA), and laboratory prepared de-ionized water are used to form polysulfone supports. Chemicals used in polyamide thin film formation include monomers 1,3-diamino benzene or *m*-phenylenediamine (MPD) and 1,3,5-benzene tricarboxylic acid chloride or trimesoyl chloride (TMC) as well as aqueous solution additives triethyl amine, TEA (liquid, 99.5%; Sigma–Aldrich), and (+)-10-champhor sulfonic acid (CSA) (powder, 99.0%; Sigma–Aldrich). Hexane, heptane, and cyclohexane (Fisher Scientific, Pittsburg, PA, USA) along with a proprietary isoparaffin, Isopar G, (Gallade Chemical, Inc.; Santa Ana, CA) are the organic solvents selected for preparing TMC solutions. Hereafter, Isopar G will be referred to generically as “isopar”.

2.2. Membrane preparation

Support membranes are prepared by dissolving 18 g PSf beads in 78 mL of NMP in airtight glass bottles. The solution is agitated with a mechanical shaker for several hours to ensure complete dissolution. The support membrane casting solution, thus obtained, is spread over a commercial non-woven polyester fabric (SepRO, Oceanside, CA) taped to a glass plate with the help of a casting blade. The glass plate is immediately immersed in laboratory prepared de-ionized water acclimated to room temperature to induce phase-inversion. After 30 min the non-woven fabric supported polysulfone film is removed from the water bath and separated from the glass plate. The membrane is washed thoroughly with de-ionized water and stored in a laboratory refrigerator maintained at 5 °C.

Polyamide composite membranes are formed by immersing the polysulfone support membrane in an aqueous solution of *m*-phenylenediamine (MPD) for 15 s. Excess MPD solution

is removed from the support membrane surface using laboratory gas forced through a custom fabricated air knife at about 34.5–48.3 kPa (5–7 psi). The air knife is a PVC pipe with a 0.3175 cm (1/8 in.) wide and 25.4 cm (10 in.) long slot cut in a straight line along one side. The MPD soaked membrane appears shiny due to the layer of water on the membrane surface. The gas is applied to the wetted membrane surface until the surface appears dull and dry. The MPD saturated support membrane is then immersed into the organic solution of trimesoyl chloride (TMC) for 15 s, which results in formation of an ultra-thin polyamide film over the polysulfone support.

The resulting composite membranes are heat cured at 50 °C for 10 min (unless otherwise specified), washed thoroughly with de-ionized water, and stored in de-ionized water filled light-proof containers at 5 °C. When additives TEA and CSA are employed, 2 g of TEA and 4 g of CSA are added to 75–80 mL of de-ionized water under vigorous stirring. After complete dissolution of the TEA–CSA mixture, de-ionized water is added to provide a total solution volume of 100 mL. Finally, 2 g of MPD is added to the 100 mL TEA–CSA aqueous solution.

2.3. Monomer and solvent characterization

The partition coefficient is the ratio of MPD concentrations in organic solvent and in water after 15 s—the time over which interfacial polymerization reactions are evaluated. To obtain the partition coefficient, a solution of 2% (w/v) MPD in water is added to 50 mL of organic solvent in a separating funnel. After 15 s, the aqueous MPD solution is removed. The concentration of MPD in the aqueous solution before and after contact with the organic is determined from total organic carbon (TOC) analysis. The ratio of MPD diffusion coefficient in each organic solvent over that in water, i.e., normalized diffusivities, are calculated based on the empirical correlation of Wilke and Chang [19] for dilute solutions of nonelectrolytes. It offers insight to the relative rates of diffusion of MPD in each organic solvent.

2.4. Membrane characterization

Pure water flux and salt rejection are evaluated by standard permeation tests using laboratory de-ionized water or de-ionized water with added salts. The filtration apparatus employed is a stainless steel dead-end stirred cell (HP4750 Stirred Cell, Sterlitech Corp., Kent, WA) resting on a magnetic stir plate. The feed chamber is pressurized by nitrogen gas as depicted in Fig. 1. Permeate volume is estimated from the mass collected in a small container resting on an electronic balance. The filtration cell has a capacity of 0.350 L and effective membrane area of 13.8 cm². All tests are conducted at room temperature (~20 °C) at applied pressure of 1551 kPa (225 psi).

Sodium chloride (ACS grade, Fisher Scientific, Pittsburg, Pennsylvania, USA) and ultra-pure de-ionized water (Barnstead NanoPure, Dubuque, IA, USA) are used in all experiments. The flux is obtained from the volume of pure water (collected over 30 min) divided by the membrane area. Intrinsic water permeability ($A = J_v / \Delta P$; J_v is the volumetric permeate flux, ΔP is the applied hydraulic pressure) is determined from the

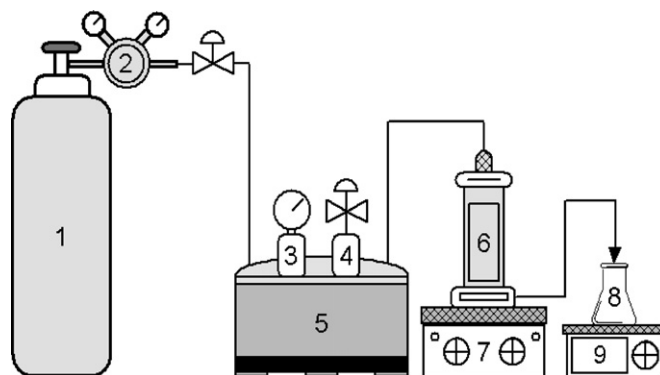


Fig. 1. Laboratory set up for evaluating RO membrane separation performance—(1) N₂ cylinder, (2) gas regulator, (3) pressure gauge, (4) pressure releasing valve, (5) feed tank, (6) membrane test cell, (7) magnetic stirrer, (8) permeate collector, and (9) weighing balance.

measured de-ionized water flux at a given externally applied hydraulic pressure. Observed salt rejection is determined by filtering 2000 ppm NaCl solution. The observed salt rejection (R_s) by each membrane is calculated from $R_s = 1 - \kappa_p / \kappa_f$, where κ_p is the measured conductivity of the total permeate volume collected and κ_f is the average of the initial and final feed conductivity. Intrinsic salt permeability (B) is determined from a re-arrangement of the solute permeability expression ($J_s = B \Delta C = J_v C_p$) where $B = J_v (1 - R_s) / R_s$ [20].

Surface morphology of membranes is visualized by scanning electron microscopy, SEM (XL30 FEG SEM, FEI Company, Hitachi, Japan) and cross-sectional morphology is visualized using transmission electron microscopy, TEM (JEOL 100CX) according to previously described methods [21]. Film thicknesses are visually characterized from TEM images using the drawing tool in MS Word. A line is drawn equal in length to the indicated scale bar on TEM images. The film thickness at ten different locations is determined from the length of a drawn line equal to the apparent film thickness. Film thicknesses are reported as an average values plus or minus the maximum deviation, such that a thickness of 100 ± 50 nm indicates a film that is on average about 100 nm thick, but ranges from ~50 to ~150 nm. These are only approximations based on a limited number of TEM images collected and analyzed.

Thin film structure is assessed by X-ray photoelectron spectroscopy (XPS) using a Kratos AXIS HS spectrometer employing a Mg KR X-ray source (1253.6 eV). The X-ray gun is operated at 10 kV and 1 mA, and the charge neutralization system is used to obtain high-resolution spectra for the insulating materials such as polymers by reducing the surface charge. The spectra are taken with the electron emission angle at 0° to give a sampling depth of <100 Å. Relative atomic concentrations and nitrogen-to-oxygen (N/O) ratios are calculated following previously published methods [12]. Theoretically, fully crosslinked and fully linear MPD–TMC films have N/O ratios of 1.0 and 0.75, respectively; however, a MPD–TMC film may possess both crosslinked and linear structures.

Quantitative surface roughness analysis of polyamide films is measured using an atomic force microscope, AFM (Digital

Table 1
Properties of solvents used to form RO membranes

Solvent (name)	ρ^a (kg/m ³)	γ^a (N/m)	μ^a (mPa s)	bp ^b (°C)	fp ^b (°C)	σ (–)	D^*c (–)
Hexane	660	18	0.300	69	–23	0.027	4.33
Heptane	680	20	0.387	98	–4	0.043	3.62
Cyclohexane	774	26	0.894	81	–18	0.072	1.44
Isopar	745	23	1.500	163	41	0.046	0.60
Water	997	72	0.893	100	n/a	1.000	1.00
Correlation coefficients							
ρ	1.00	0.98	0.37	0.10	0.34	0.95	–0.67
γ		1.00	0.20	0.00	0.22	1.00	–0.50
μ			1.00	0.84	0.83	0.13	–0.92
bp				1.00	1.00	–0.03	–0.64
fp					1.00	0.00	–0.68

^a Data obtained for 25 °C from “CRC Handbook of Chemistry and Physics,” David R. Lide, 84th Edition (2003–2004), CRC Press.

^b Data obtained from MSDS sheets provided by solvent supplier.

^c Relative diffusivity for isopar determined as $D^* = \mu_{\text{water}}/\mu_{\text{solvent}}$.

Instruments-Multimode 3, Santa Barbara, CA, USA), equipped with standard silicon nitride cantilever (MikroMasch, Portland, OR, USA). The estimated tip radius is less than 10 nm, cantilever length is 125 μm and force constant of 5 N/m. Air-dried membrane samples are fixed on a specimen holder and 10 $\mu\text{m} \times 10 \mu\text{m}$ areas are scanned by tapping mode in air. Roughness is reported in terms of the measured root mean square (RMS \approx standard deviation in height values recorded by AFM [22]) roughness and relative surface area (Δ = actual surface area divided by the planar area [23]).

Surface hydrophilicity of all membranes is evaluated from the average equilibrium sessile drop contact angles of de-ionized water on dried membrane surfaces. Membranes are dried overnight at room temperature in a desiccator. At least twelve equilibrium contact angles are obtained for each membrane, where the average of left and right contact angles defines the equilibrium contact angle. The minimum and maximum equilibrium angles are dropped. Average membrane contact angles and standard deviations are determined from the remaining data. A modified form of the Young–Dupre equation is used to evaluate relative hydrophilicity of membranes by the solid–liquid interfacial free energy. In our modification, we correct for the increase in surface area due to roughness, a.k.a., the relative surface area, as suggested by Wenzel [23].

The solid–liquid interfacial free energy is determined from $-\Delta G_{\text{SL}} = \gamma_{\text{L}}[1 + \cos\theta/\Delta]$, where θ is the average contact angle and γ_{L} ($=72.8 \text{ mJ/m}^2$ for pure water at 25 °C) is the liquid surface tension. For a perfectly smooth surface, the solid–liquid interfacial free energy ranges from γ_{L} for measured contact angle of 90° up to $2\gamma_{\text{L}}$ for measured contact angle of 0°; hence, a larger value of $-\Delta G_{\text{SL}}$ suggests a more hydrophilic surface. However, for rough surfaces where the contact angle is below 90°, the measured contact angle is smaller than it would be on a smooth surface comprised of the same material. The opposite is true for non-wetting materials with measured contact angles greater than 90°. The $-\Delta G_{\text{SL}}$ values reported herein are the “surface area corrected” solid–liquid interfacial free energy, which is better representation of a film’s hydrophilicity than the observed contact angle.

3. Results and discussion

3.1. Relevant physicochemical properties of organic solvents

Selected physical properties of organic solvents and correlation coefficients for boiling point (bp), flash point (fp), partition coefficient (σ), and relative diffusivity (D^*) with respect to solvent viscosity, density, and surface tension are also reported in Table 1. Correlations are classified as strong, moderate, and weak for coefficients greater than 0.85, between 0.85 and 0.4, and less than 0.4, respectively. Boiling points and flash points correlate most significantly with solvent viscosity. Isopar is clearly the most stable solvent with dramatically higher boiling and flash points. The relatively low boiling points of hexane, heptane, and cyclohexane suggest curing at low temperatures and short times should be adequate, whereas isopar will require higher temperatures and longer times.

Density, surface tension, and viscosity clearly influence diffusion and partitioning of the MPD monomer in the

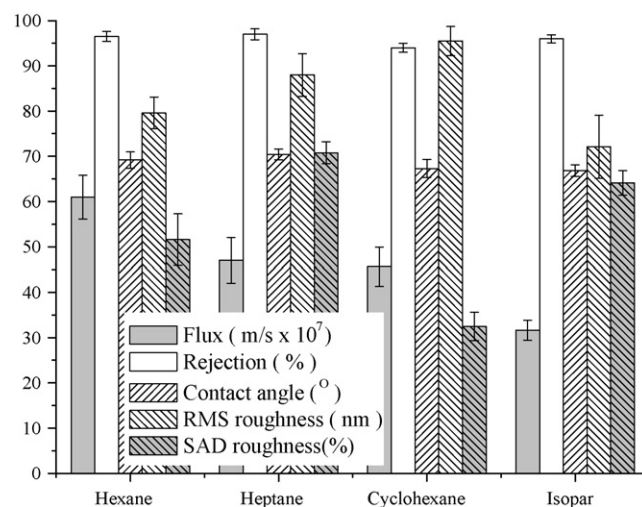


Fig. 2. Properties of RO membranes formed using different organic solvents.

organic phase. Diffusivity of MPD in the organic solvents is observed from highest to lowest according to hexane > heptane > cyclohexane > isopar, which strongly correlates (negatively) with solvent viscosity. Information needed to quantify the exact diffusivity of isopar is not available because of its proprietary composition; therefore, the relative diffusion coefficient

reported in Table 1 is the ratio of water viscosity to that of isopar. The partition coefficient provides insights into the relative availability of MPD and the thickness of the reaction zone in each organic solvent [6,24]. Solubility of MPD in the organic solvents decreases as cyclohexane > heptane ~ isopar > hexane, which strongly correlates with surface tension.

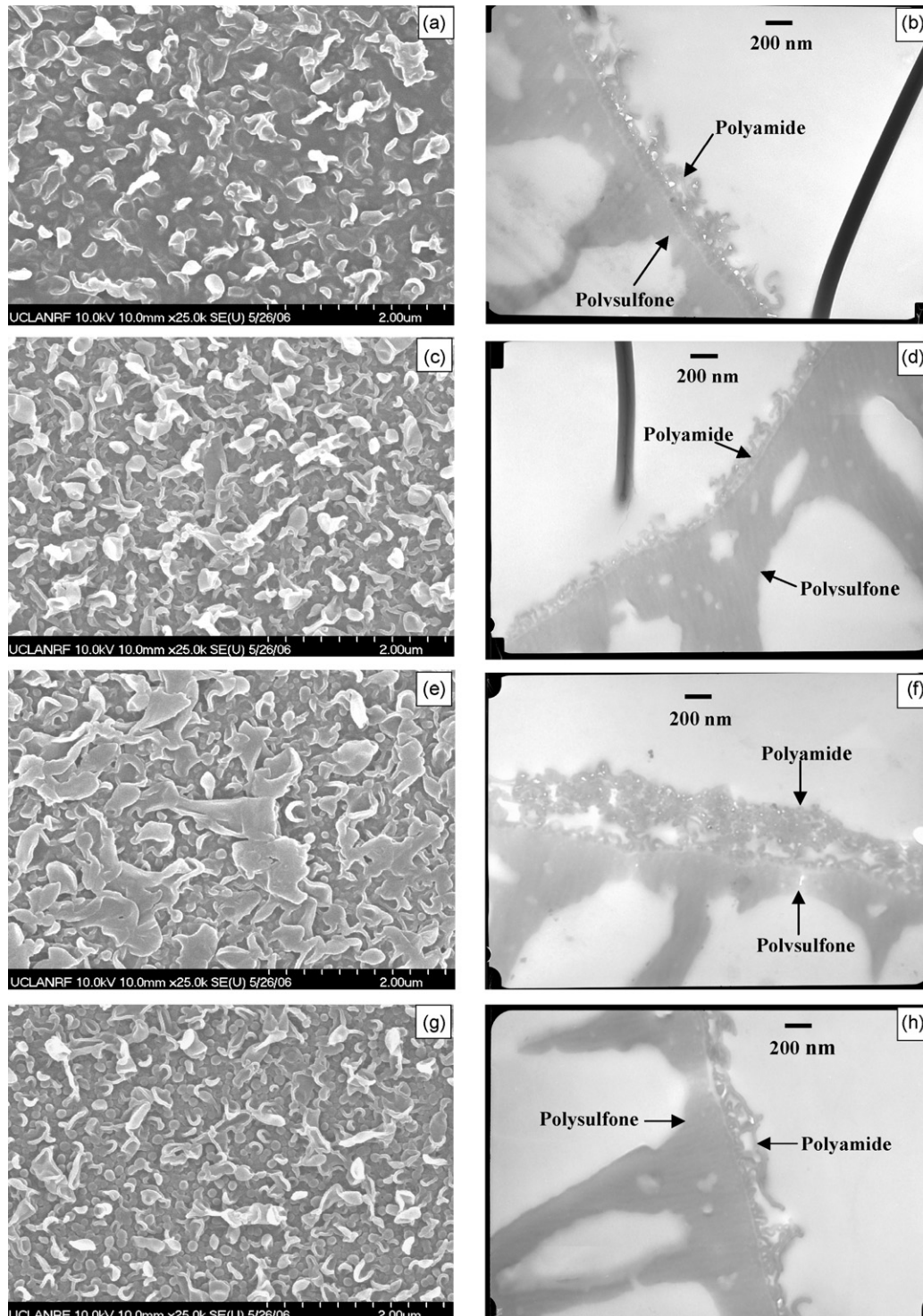


Fig. 3. SEM and TEM images of RO membranes prepared in (a, b) hexane, (c, d) heptane, (e, f) cyclohexane, and (g, h) isopar.

3.2. Properties of membranes formed in different organic solvents

Experimentally determined values of pure water flux, salt rejection, contact angle, and surface roughness (RMS and SAD) are plotted in Fig. 2 with average values indicated by the bar height and standard deviation of measured values indicated by the error bars. Observed water flux decreases as hexane > heptane ~ cyclohexane > isopar, whereas observed salt rejection decreases in order of heptane > hexane > isopar > cyclohexane. Observed contact angle decreases in order of heptane ~ hexane > cyclohexane ~ isopar. Measured RMS roughness decreases in order of cyclohexane > heptane > hexane > isopar, while SAD values decrease as heptane > isopar > hexane > cyclohexane.

Representative SEM and TEM images of membranes prepared using each organic solvent are provided in Fig. 3. In the SEM images of Fig. 3(a, c, e, and g), the rugose surface morphology characteristic of MPD–TMC films is evident. The hexane, heptane, and isopar-based membranes are similar, but the cyclohexane-based membrane exhibits more “leaf-like” folds on its surface. In the TEM images of Fig. 3(b, d, f, and h), the films are viewed in cross-section. By visual inspection, film thicknesses of the membranes decrease in the order of cyclohexane > hexane > isopar > heptane. Image analysis suggests film thicknesses on the order of 350 ± 100 , 200 ± 100 , 150 ± 100 , and 100 ± 50 nm for cyclohexane, hexane, isopar, and heptane, respectively.

Observed properties are of practical interest, but do not give rise to mechanistic understanding of the impacts of organic solvents on intrinsic membrane properties. For example, flux and rejection are not intrinsic properties of a membrane because they are influenced by mass transfer and operating conditions, whereas solvent and solute permeability are (in principle) intrinsic properties of a membrane. In addition, the surface area corrected interfacial free energy is a better measure of hydrophilicity than contact angle. Average values of pure water permeability (A), salt permeability (B), membrane hydrophilicity ($-\Delta G_{SL}$), apparent film thickness (δ_{film}), extent of crosslinking (N/O), surface roughness (RMS), and relative

surface area (Δ) for membranes prepared using different organic solvents are reported in Table 2.

Water permeability decreases in the same order as the observed flux, hexane > heptane ~ cyclohexane > isopar. However, salt permeability decreases in the order of cyclohexane > hexane > heptane > isopar, which is inconsistent with observed salt rejection. Salt rejection may appear higher for more water permeable membranes due to the higher water flux produced at the fixed pressure used in permeation tests; however, the salt permeability is relatively independent of operating conditions. Hydrophilicity decreases in the order of cyclohexane > isopar ~ hexane > heptane, which is different from observed contact angles (isopar ~ cyclohexane < hexane ~ heptane). Film thickness decreases in order of cyclohexane > hexane > isopar > heptane and extents of crosslinking decreases in order of hexane ~ heptane > isopar > cyclohexane. The low boiling points of hexane and heptane may lead to near complete crosslinking because the membranes were cured at sufficiently high temperature to completely dehydrate the films.

Correlation coefficients for each intrinsic membrane property are calculated for the relative solubility (σ) and diffusivity (D^*) of MPD in each solvent. Pure water permeability is strongly correlated with MPD diffusivity and moderately (negatively) correlated with MPD solubility. The former relationship is expected based on the general belief that MPD–TMC interfacial polymerization reactions are diffusion limited. However, water permeability is weakly correlated with film thickness (positively), film hydrophilicity (negatively), surface roughness (positively), and surface area (negatively), but moderately correlated with crosslinking (positively). These relationships contradict the general perception that permeability is directly proportional to hydrophilicity and roughness and inversely proportional to film thickness and crosslinking. Overall, more water permeable films are formed by enhancing MPD diffusivity and reducing MPD solubility, which also tends to increase crosslinking.

Salt permeability is moderately correlated with MPD solubility and virtually uncorrelated with MPD diffusivity. Salt permeability is also strongly correlated with hydrophilicity

Table 2
Correlation of intrinsic membrane properties with MPD diffusivity and solubility

Solvent (name)	A ($\mu\text{m}/\text{bar s}$)	B ($\mu\text{m}/\text{s}$)	$-\Delta G_{SL}$ (mJ/m^2)	δ_{film} (nm)	N/O (–)	RMS (nm)	Δ (–)
Hexane	3.93	0.221	89.9	200	1.01	79.6	1.52
Heptane	3.03	0.145	87.1	100	1.01	88.0	1.71
Cyclohexane	2.94	0.291	94.0	350	0.89	95.5	1.33
Isopar	2.04	0.132	90.3	150	0.92	72.1	1.64
Correlation coefficients							
σ	–0.46	0.51	0.71	0.68	–0.84	0.65	–0.59
D^*	0.89	0.03	–0.55	–0.31	0.91	0.13	0.20
A	1.00	0.45	–0.11	0.14	0.63	0.29	–0.26
B		1.00	0.80	0.94	–0.39	0.69	–0.97
$-\Delta G_{SL}$			1.00	0.95	–0.83	0.37	–0.93
δ_{film}				1.00	–0.67	0.58	–0.99
N/O					1.00	–0.18	0.58
RMS						1.00	–0.56

(positively), film thickness (positively), and surface area (negatively); it is moderately correlated with surface roughness and weakly (negatively) correlated with crosslinking. Therefore, salt passage is reduced by decreasing MPD solubility, which is consistent with increasing water permeability.

Hydrophilicity, a key property for fouling resistance, is moderately correlated with MPD solubility (positively) and diffusivity (negatively), but strongly co-correlated with film thickness (positive), crosslinking (negative), and surface area (negative). Apparent film thickness is moderately correlated with MPD solubility and weakly (negatively) correlated with MPD diffusivity. Film thickness is also strongly correlated with surface area (negatively), hydrophilicity (positively), and salt permeability (positively). Crosslinking is strongly correlated with both MPD solubility (negatively) and diffusivity (positively).

The relative surface roughness correlates weakly-to-moderately with MPD solubility and negligibly with MPD diffusivity. The characteristic size of surface roughness features (RMS) correlates moderately with MPD solubility, while the relative surface area correlates moderately (negatively) with MPD solubility. The latter correlation reinforces the potential mechanistic connection between film structure (crosslinking) and effective membrane surface area pointed out previously by others [25,12,26,13]. Increasing MPD solubility tends to increase hydrophilicity, film thickness, and surface roughness, while decreasing surface area and crosslinking.

Consider the following scenarios based on MPD solubility and diffusivity in (1) hexane and heptane, (2) heptane and isopar, and (3) heptane and cyclohexane. In the first scenario, diffusivity of MPD in both solvents is similar, but solubility of MPD in hexane is half that of heptane. The hexane film is thicker, but both permeability coefficients (A and B) are larger; hence, high MPD solubility produces an intrinsically more permeable film (for both salt and water). In the second scenario, solubilities of MPD in heptane and isopar are similar, but diffusivity of MPD in heptane is six times greater. The isopar film is thicker, its water permeability is lower, but its salt permeability is similar; hence, high MPD diffusivity enhances water, but not salt permeability. In the third scenario, heptane has about half the solubility and double the diffusivity of cyclohexane. Heptane produces a thinner film with about the same water permeability (as cyclohexane), but half the salt permeability; hence, higher MPD solubility and lower diffusivity of cyclohexane produces a thicker film with a potentially looser structure.

The lack of correlation between film thickness and permeability suggest the entire film thickness (as depicted by TEM images) may not contribute to separation. In a series of theoretical and experimental studies, Freger and co-workers suggests the existence of a “dense inner barrier layer” responsible for separation [27,6,24]. Our experimental results provide further support for this idea. When SEM and TEM images are viewed together, some of the leaf-like folds (in SEM surface images) appear to bridge over top of another film layer below (in TEM images)—forming a discontinuous nano-porous coating layer. These leaf-like folds clearly do not contribute directly to permeation. Water and solutes must flow around the leaf-like masses

of MPD–TMC polymer with separation occurring at an inner barrier layer. The presence of a nano-porous layer covering the actual separation layer could hinder solute diffusion and, perhaps, lead to enhanced concentration polarization [28]. This effect would be most pronounced on the cyclohexane-based membrane with its relatively thick nano-porous coating layer.

Some points of caution. Our results show only a small range of variability in measured contact angles and surface roughness. Further, we lack rigorous methods to properly assess the impact of surface roughness on measured contact angles. In addition, differences in measured contact angles may not be purely due to membrane structural features. Residual solvent entrapped within the films can produce unrealistically high water contact angles. Although membranes were rinsed thoroughly with de-ionized water after curing, differences in film layer hydrophilicity may be underestimated for the higher boiling point solvents (like isopar) because these solvents may not be completely removed without some additional chemical treatments.

3.3. Properties of membranes formed with additive TEA–CSA

Use of additives in monomer solutions can influence the rate and extent of interfacial polymerization as well as the extent of crosslinking [12]. Properties of polyamide films formed with TEA–CSA added to the aqueous-MPD reaction solution are plotted in Fig. 4. These data represent average changes in pure water permeability, salt permeability, contact angle, and surface roughness relative to the membrane formed without TEA–CSA in the same solvent. In all the cases, pure water permeability dramatically increases, salt rejection is practically unchanged, contact angle is slightly reduced, and roughness is significantly reduced by TEA–CSA addition.

SEM and TEM images from hexane and isopar based membranes prepared using with the TEA–CSA additives are provided in Fig. 5. Membrane surface features appear more nodular when TEA–CSA is present compared to the ridge-and-valley mor-

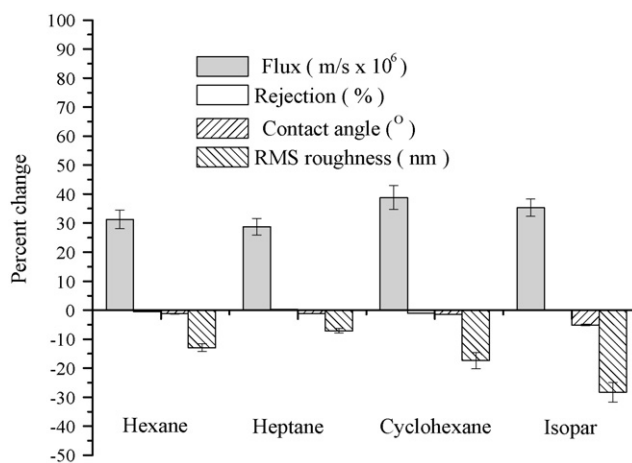


Fig. 4. Percent change in properties of RO membranes formed with TEA–CSA added to aqueous MPD solution. Data are plotted as (“value obtained with TEA–CSA” – “value obtained without TEA–CSA”) divided by “value obtained without TEA–CSA”.

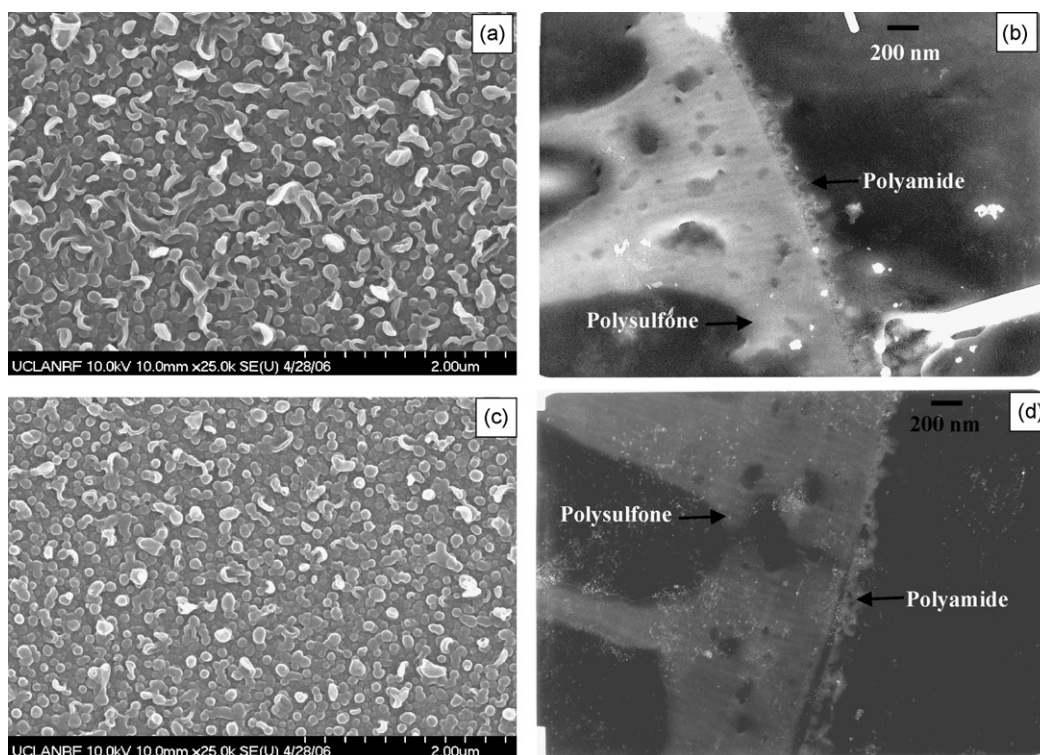


Fig. 5. SEM and TEM images of RO membranes prepared in (a, b) hexane, (c, d) isopar with TEA–CSA added to the aqueous-MPD solution.

phology of membranes formed without TEA–CSA (Fig. 3(a and g)). The nodular morphology is measurably smoother than the ridge-and-valley morphology according to AFM surface roughness analyses. Cross-section TEM images of hexane and isopar based membranes prepared with TEA–CSA looked thinner and smoother than without TEA–CSA membranes (Fig. 3(b and h)).

In principle, TEA in the aqueous solution might compete with MPD partitioning, diffusion, and reaction with TMC; however, the reactivity of TMC with MPD is generally much higher than tertiary amines such as TEA [2]. It is more likely that TEA acts as a catalyst, accelerating the MPD–TMC reaction by neutralizing HCl produced during amide formation. Thinner, more crosslinked MPD–TMC films appear to form, and hence, membrane permeability increases without a loss of salt rejection. Other higher order amines perform a similar role, such as trimethyl amine or piperazines, but experience has shown that TEA is most effective. Addition of CSA is generally believed to protect the microporous skin layer of the support membrane from annealing during curing [2], although (to our knowledge) the mechanism has not been elucidated in published literature. This is especially important when high boiling point solvents are used because they require high temperature curing.

3.4. Properties and morphology of RO membranes formed at different temperatures

The kinetics of MPD–TMC film formation are investigated here by varying the TMC-organic solution temperature during the interfacial polymerization. Isopar is used for these analyses because it is sufficiently non-volatile across the range of tem-

peratures evaluated. Also, TEA–CSA is added to the MPD in aqueous solution to produce membranes with superior baseline performance and because heat curing is performed at 75 °C for 10 min.

Observed water permeability, salt rejection, hydrophilicity, and roughness data are presented in Fig. 6. As the temperature of isopar increases, permeate flux increases, salt rejection decreases, contact angle increases, surface roughness increases, and surface area decreases. Density, surface tension, and viscosity of isopar decrease as temperature increases;

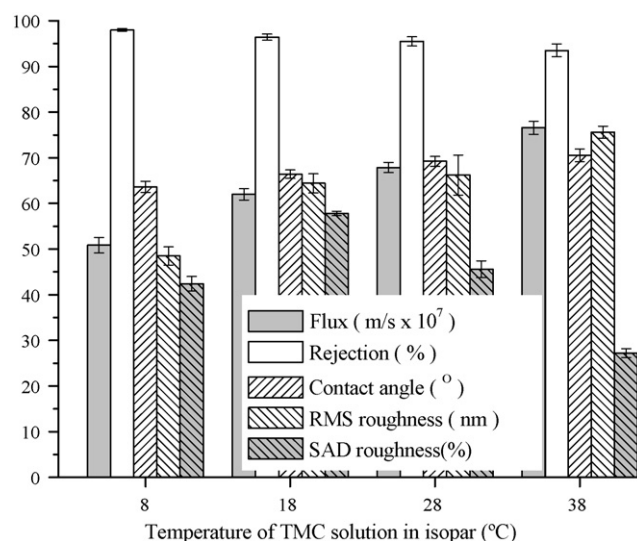


Fig. 6. Properties of RO membranes formed from TMC-isopar solutions at different temperatures.

hence, MPD solubility and diffusivity in isopar increase with temperature.

Following the logic developed above, higher MPD solubility (in isolation) should produce thicker, less crosslinked films

(more MPD is available to form the polymer, but hydrolysis of TMC inhibits crosslinking), while higher MPD diffusivity (in isolation) should produce thinner, more crosslinked films (contiguous film forms more quickly, terminating the reaction, and

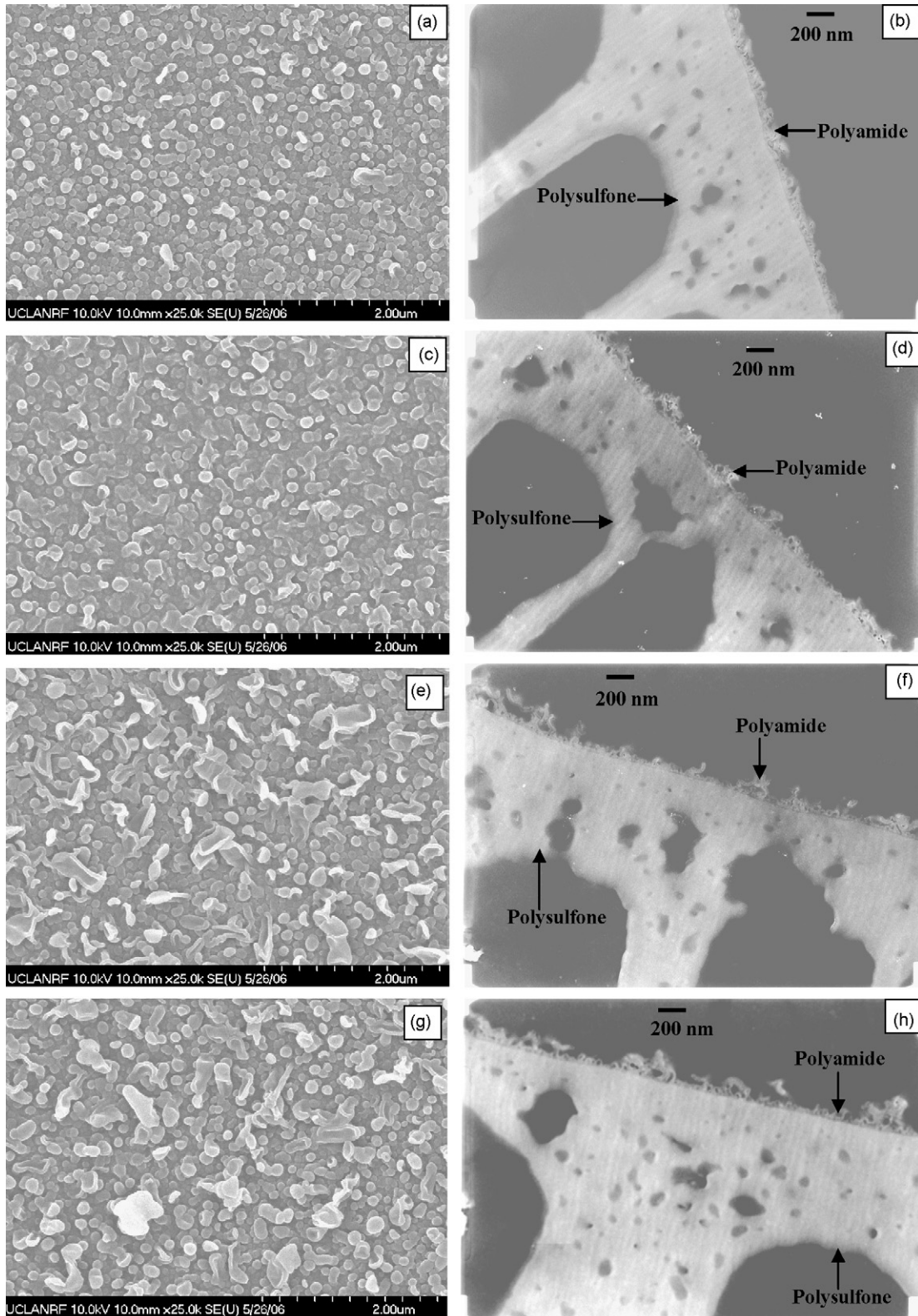


Fig. 7. SEM and TEM images of RO membranes prepared in isopar at (a, b) 8, (c, d) 18, (e, f) 28, and (g, h) 38 °C.

monomers can more easily form multiple amide linkages). The increase in contact angle (with increasing temperature) probably results from the decrease in surface area. However, as the polycondensation reaction between amine and acid chloride is exothermic, the reaction rate should decrease with increasing temperature—ultimately increasing the extent of crosslinking, which is supported by the large increase in flux and slight decrease in rejection.

Electron microscope (SEM and TEM) images of membranes are provided in Fig. 7 formed at different isopar-TMC solution temperatures. The membranes prepared at lower temperature (8 °C) contain many tightly packed, small nodular structures. With increasing isopar temperature, the membranes develop increasingly rough, ridge-and-valley morphology—closer to hexane and heptane based membranes depicted in Fig. 5. Relatively fewer, but larger “tufts” appear as temperature increases, and the interconnecting film layer between is thinner. Increasing TMC solution temperature produces thinner, rougher, more permeable films. However, the apparent correlation between surface roughness and water flux may be coincidental because the film layer thickness (between roughness features) and structure (crosslinking) are the most important factors in determining membrane permeability.

3.5. Properties of membranes cured at different temperatures and times

Heat curing is often required to facilitate the removal of residual organic solvent from nascent polyamide thin films and to promote additional crosslinking by dehydration of unreacted amine and carboxyl groups. Optimal curing temperatures and times vary for different solvents depending on the solvent evaporation rate (i.e., boiling point). We evaluate the impacts of curing temperature and time on separation performances of composite MPD–TMC membranes formed using the four organic solvents. All other preparation conditions are identical to membranes formed in Section 3.4.

Separation performances of membranes cured at different temperatures are evaluated for a fixed curing time of 10 min. Water flux and salt rejection data for each curing temperature are plotted in Figs. 8 and 9, respectively. For low boiling point solvents (hexane and cyclohexane), flux increases in the range of 45–60 °C, but drops off above 75 °C. This contrasts with the high boiling solvents (heptane and isopar), which exhibit increasing flux through 90 °C. Once evaporation of organic solvents from the membrane surface is complete, evaporation

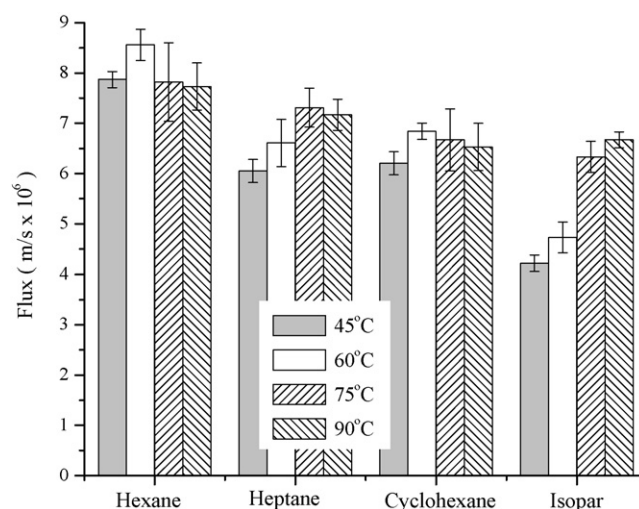


Fig. 8. Impacts of curing temperature on water flux for RO membranes prepared in hexane, heptane, cyclohexane, and isopar.

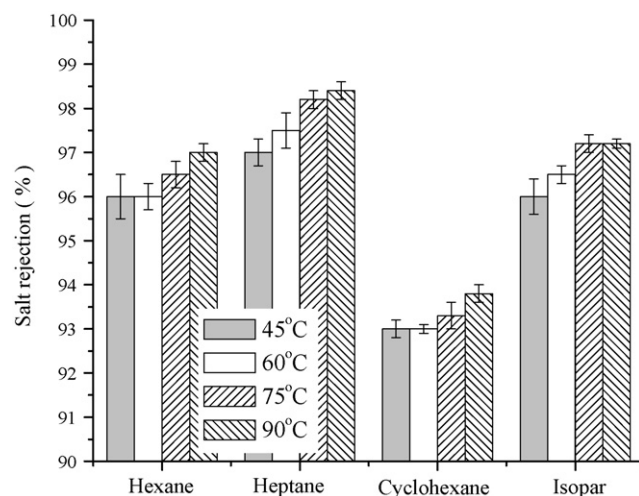


Fig. 9. Impacts of curing temperature on salt rejection for RO membranes prepared in hexane, heptane, cyclohexane, and isopar.

of bound water inside the membrane occurs. At higher temperatures, there is a chance of pore shrinkage in the support membranes. The decrease in flux for hexane and cyclohexane membranes at 90 °C could be due to this. However, salt rejection also increases with increasing curing temperature, which suggests additional crosslinking occurred. Similar results are reported for hexane-based polyamide membranes formed with different coating conditions and polysulfone supports [16].

Table 3
Effect of curing temperature on RO membranes formed in heptane

Cure temp (°C)	A (μm/bar s)	B (μm/s)	−ΔG _{SL} (mJ/m ²)	RMS (nm)	Δ (–)
45	3.90	0.187	92.4	85	1.51
60	4.26	0.169	89.1	73	1.62
75	4.71	0.134	91.3	59	1.38
90	4.62	0.117	89.1	104	1.51
Correlation coefficients					
Temp	0.91	−0.99	−0.60	0.27	−0.30

Table 4
Effect of curing time on RO membrane performance

Cure temp (°C)	Cure time (min)	Hexane		Isopar	
		A ($\mu\text{m}/\text{bar s}$)	B ($\mu\text{m}/\text{s}$)	A ($\mu\text{m}/\text{bar s}$)	B ($\mu\text{m}/\text{s}$)
45	2	4.73	0.306	1.98	0.145
	10	5.07	0.328	2.72	0.176
	18	5.00	0.451	3.20	0.207
90	2	5.10	0.262	2.92	0.140
	10	4.98	0.239	4.30	0.192
	18	4.72	0.266	4.37	0.217
Correlation coefficients					
45		0.75	0.93	0.99	1.00
90		−0.98	0.14	0.89	0.98

Additional properties of heptane-based membranes are given in Table 3. Water and salt permeability correlate almost perfectly with temperature, while hydrophilicity and roughness correlate moderately and weakly with temperature, respectively. Changes in hydrophilicity are subtle and it is not clear exactly how structure and morphology conspire to produce the measured contact angle. Regardless, the trend is clear. As curing temperature increases, water permeability increases, while salt permeability and hydrophilicity decrease—consistent with loss of residual solvent and gain in crosslinking. Membrane surface roughness decreases with increasing curing temperature up to 75 °C, but then increases dramatically (especially RMS) at 90 °C. The evaporation of excess surface organic solvent takes place more rapidly when the temperature of the curing approaches the boiling point of the solvent. Hence, the rougher surface formed by curing at 90 °C temperature could be due to the violence of the rapidly volatilizing solvent.

Overall, the best RO membrane was obtained with heptane as the organic solvent at a curing temperature of 75 °C. It had the highest water permeability and lowest roughness with excellent salt rejection (98.2%). Only subtle changes in hydrophilicity were observed as a result of curing. Since the membranes were immediately placed in the oven after their exposure to the TMC solution, additional hydrolysis of unreacted acyl groups (−COCl) of TMC may stop more quickly at higher curing temperatures because of more rapid film dehydration; hence, more crosslinking occurs and hydrophilicity decreases.

The separation performance of MPD–TMC composite membranes is further evaluated here across a range of curing times. Hexane and isopar are the solvents used at curing temperatures of 45 and 90 °C. Water flux and salt rejection are reported in Table 4. At 45 °C for 2 min, evaporation of both solvents from the film is incomplete. Upon immersion in de-ionized water, an oily residue released from the surface of the membranes. Permeability of these membranes is relatively poor because some solvent remains in the film. At 45 °C, membrane performance declined for hexane after 10 min of curing, but the isopar-based membrane continued to improve through 18 min of curing. At 90 °C, about 2 min is adequate for hexane, whereas at least 10 min is required for isopar. With increasing curing time, complete evaporation of organic solvents from the membranes is achieved and the permeability is higher. Curing significantly longer than the

minimum time needed to remove the solvent also may result in shrinkage or annealing of support membrane pores, which decreases water permeability.

4. Conclusions

Generally, RO membrane water permeability and salt rejection increase with increasing MPD diffusivity and decreasing MPD solubility. If higher MPD diffusivity is accomplished by changing to an organic solvent also giving higher MPD solubility, films exhibit higher water flux, salt passage, thickness, and roughness, but less crosslinking. If higher MPD diffusivity is accomplished by heating an organic solvent with low MPD solubility, films exhibit higher water flux, salt passage, crosslinking, and roughness. Curing at higher temperatures is needed to fully remove high boiling point solvents. Adding the salt of TEA and CSA to the aqueous-MPD solution increases MPD–TMC performance by inhibiting amine protonation and acid chloride hydrolysis, and possibly by protecting the support membrane during high temperature curing.

Perhaps the most important conclusion from this study is that MPD–TMC film thickness and morphology are not intrinsically related to water permeability. The lack of correlation between film thickness and water permeability suggest the entire film thickness does not determine the pressure drop across composite RO membranes. Rather, permeation may occur at a “dense inner barrier layer” and the visible surface morphology is an unfortunate byproduct of the polymerization reaction. Interestingly film thickness, surface area, and hydrophilicity strongly correlate with salt permeability, which suggests mass transfer may be influenced by surface morphology. Finally, reaction and curing conditions that produce optimal separation performance tend to produce relatively rough, hydrophobic membrane surfaces, which presents an unfortunate conundrum for membrane scientists hoping to produce high performance, fouling resistant RO membranes via traditional polymer chemistry routes.

Disclosure statement

The corresponding author has a financial interest in one of the project co-sponsors, NanoH₂O Inc., through stock ownership and consulting activities.

Acknowledgements

The authors are grateful for the financial support received from the California NanoSystems Institute (CNSI) and NanoH₂O Inc. The authors are also grateful to Prof. Yang Yang and Xu Zheng in the Department of Materials Science and Engineering at UCLA for performing the XPS analyses.

References

- [1] S.H. Chen, D.J. Chang, M.R. Liou, C.S. Hsu, S.S. Lin, Preparation and separation properties of polyamide nanofiltration membrane, *J. Appl. Polym. Sci.* 83 (2002) 1112.
- [2] R.J. Petersen, Composite reverse-osmosis and nanofiltration membranes, *J. Membr. Sci.* 83 (1993) 81.
- [3] M.M. Chau, W.G. Light, A.X. Swamikannu, Chlorine-tolerant, thin-film composite membrane, US Patent 5,271,843 (1993).
- [4] H. Hachisuka, K. Ikeda, Reverse osmosis composite membrane and reverse osmosis treatment method for water using the same, US Patent 6,413,425 (2002).
- [5] S. Verissimo, K.V. Peinemann, J. Bordado, Thin-film composite hollow fiber membranes: an optimized manufacturing method, *J. Membr. Sci.* 264 (2005) 48.
- [6] V. Freger, Kinetics of film formation by interfacial polycondensation, *Langmuir* 21 (2005) 1884.
- [7] P.W. Morgan, Interfacial polymerization without stirring, in: *Condensation Polymers: by Interfacial and Solution Methods*, Interscience Publishers, New York, NY, 1965, pp. 19–64 (Chapter 2).
- [8] P.W. Morgan, S.L. Kwolek, Interfacial polycondensation 2. Fundamentals of polymer formation at liquid interfaces, *J. Polym. Sci. Pt. A: Polym. Chem.* 34 (1996) 531.
- [9] E.L. Wittbecker, P.W. Morgan, Interfacial polycondensation 1, *J. Polym. Sci. Pt. A: Polym. Chem.* 34 (1996) 521.
- [10] I.C. Kim, J. Jegal, K.H. Lee, Effect of aqueous and organic solutions on the performance of polyamide thin-film-composite nanofiltration membranes, *J. Polym. Sci. Pt. B: Polym. Phys.* 40 (2002) 2151.
- [11] M. Hirose, K. Ikeda, Method of producing high permeable composite reverse osmosis membrane, US Patent 5,576,057 (1996).
- [12] S.H. Kim, S.Y. Kwak, T. Suzuki, Positron annihilation spectroscopic evidence to demonstrate the flux-enhancement mechanism in morphology-controlled thin-film-composite (TFC) membrane, *Environ. Sci. Technol.* 39 (2005) 1764.
- [13] S.Y. Kwak, S.G. Jung, S.H. Kim, Structure–motion–performance relationship of flux-enhanced reverse osmosis (RO) membranes composed of aromatic polyamide thin films, *Environ. Sci. Technol.* 35 (2001) 4334.
- [14] M.A. Kuehne, R.Q. Song, N.N. Li, R.J. Petersen, Flux enhancement in TFC RO membranes, *Environ. Prog.* 20 (2001) 23.
- [15] J.E. Tomaschke, Interfacially synthesized reverse osmosis membrane containing an amine salt and processes for preparing the same, US Patent 4,872,984 (1989).
- [16] A.P. Rao, N.V. Desai, R. Rangarajan, Interfacially synthesized thin film composite RO membranes for seawater desalination, *J. Membr. Sci.* 124 (1997) 263.
- [17] A.P. Rao, S.V. Joshi, J.J. Trivedi, C.V. Devmurari, V.J. Shah, Structure–performance correlation of polyamide thin film composite membranes: effect of coating conditions on film formation, *J. Membr. Sci.* 211 (2003) 13.
- [18] W.E. Mickols, Composite membrane and method for making the same, US Patent 6,562,266 (2003).
- [19] C.R. Wilke, P. Chang, Correlation of diffusion coefficients in dilute solutions, *AIChE J.* 1 (1955) 264.
- [20] M. Mulder, *Basic Principles of Membrane Technology*, second ed., Kluwer Academic Publishers, Dordrecht, NL, 1991, pp. 416–424.
- [21] B.H. Jeong, E.M.V. Hoek, Y. Yan, A. Subramani, X. Huang, A.K. Ghosh, A. Jawor, Interfacial polymerization of thin film nanocomposites: a new concept for reverse osmosis membranes, *J. Membr. Sci.* 294 (2007) 1.
- [22] E.M.V. Hoek, S. Bhattacharjee, M. Elimelech, Effect of membrane surface roughness on colloid-membrane DLVO interactions, *Langmuir* 19 (2003) 4836.
- [23] R.N. Wenzel, Surf. Rough. Contact Angle 53 (1949) 1466.
- [24] V. Freger, S. Srebnik, Mathematical model of charge and density distributions in interfacial polymerization of thin films, *J. Appl. Polym. Sci.* 88 (2003) 1162.
- [25] C.K. Kim, J.H. Kim, I.J. Roh, J.J. Kim, The changes of membrane performance with polyamide molecular structure in the reverse osmosis process, *J. Membr. Sci.* 165 (2000) 189.
- [26] S.Y. Kwak, D.W. Ihm, Use of atomic force microscopy and solid-state NMR spectroscopy to characterize structure–property–performance correlation in high-flux reverse osmosis (RO) membranes, *J. Membr. Sci.* 158 (1999) 143.
- [27] V. Freger, Nanoscale heterogeneity of polyamide membranes formed by interfacial polymerization, *Langmuir* 19 (2003) 4791.
- [28] E.M.V. Hoek, M. Elimelech, Cake-enhanced concentration polarization: a new fouling mechanism for salt-rejecting membranes, *Environ. Sci. Technol.* 37 (2003) 5581.